A new approach to investigate leakage current mechanisms in infrared photodiodes from illuminated current-voltage characteristics

Vishnu Gopal[a)]
Institute of Defence Scientists and Technologists, CFEES Complex, Brig. S. K. Majumdar Marg, Delhi 110054, India

(Received 31 July 2014; accepted 13 August 2014; published online 25 August 2014)

This paper presents a new approach to investigate leakage current mechanisms in infrared photodiodes from the illuminated current–voltage characteristics. The example of mid-wave mercury cadmium telluride photodiodes is presented to illustrate the new approach. The new method is suitable for evaluating diodes in an array environment as advance knowledge of any of the material or device parameters are not required. The thermal saturation current is estimated from the observed open circuit voltage and zero-bias current (photo-current) of the diode. The ohmic shunt resistance is estimated from the observed maximum dynamic impedance of the diode. The experimentally observed reverse bias diode current in excess of thermal current, photo-current, and ohmic shunt current is reported to be best described by an exponential function of the type, $I_{excess} = I_{r0} + K_1 \exp(K_2 V)$, where I_{r0}, K_1, and K_2 are fitting parameters and V is the applied bias voltage. Our investigations reveal a close link between the excess current and the sources of ohmic currents in the diode. Exponential growth of excess current with the applied bias voltage has been interpreted as an indication of soft breakdown of the diodes. © *2014 AIP Publishing LLC*.
[http://dx.doi.org/10.1063/1.4893899]

I. INTRODUCTION

Photovoltaic detector arrays fabricated from narrow band gap mercury cadmium telluride (HgCdTe) semiconductor material constitute the heart of modern thermal imaging systems operating in 3–5 μm and 8–12 μm atmospheric windows. The ultimate performance of these advanced systems gets limited by the dynamic impedance of the diodes in the array. It is well known that the dynamic impedance of the diode determines the noise of the detector and the injection efficiency of the signal in to readout circuit if the detector is the part of a focal plane array. High dynamic impedance of the diodes in the array leads to lower noise level and high injection efficiency. Investigations of excess leakage currents, which influence the diode's dynamic impedance continues to be, thus, an important activity for realising high performance infrared arrays. The present practice of investigating the leakage current mechanisms is based on the analyses of the measured dark electrical characteristics (current-voltage and/or dynamic resistance-voltage) of the diodes by a computer fitting programme or analytical modelling[1–5] using the known theory of each of the leakage current mechanisms. The present paper presents a new approach to investigate the excess leakage current mechanisms from the illuminated characteristics in a mid-wave HgCdTe photovoltaic detector array.

II. EXPERIMENTAL

An area array consisting of n^+ on p diodes was investigated in this experiment. The diodes were fabricated by boron ion implantation using standard photolithographic process on a p-type mercury cadmium telluride ($Hg_xCd_{1-x}Te$, $x = 0.295$) epitaxial layer grown by LPE on a lattice matched CdZnTe substrate. The dimension of each diode in the array was $40 \times 70\ \mu m^2$. An evaporated CdTe film on the array was used for its passivation.

The current–voltage characteristics of several diodes in the area array were measured by mounting the array on a cold stage. The cold mount was maintained in a vacuum environment by surrounding it with a suitable metallic cylinder connected to a vacuum pump. In this setup, the diodes remained illuminated by the background radiation from the outer metallic walls of the measurement setup. No effort was made to provide an effective cold shield. However, partial cold shielding was present due to the design of the electrical probe and cold mount that had relative motion to each other to probe multiple detectors in the given array. All the experimental activity was carried out by the scientists of Infrared division in Solid State Physics Laboratory Delhi. The measured current–voltage (I–V) characteristics were made available to the author for the analysis of leakage current mechanisms in the fabricated arrays.

III. PHYSICAL MODEL

In HgCdTe junctions, the known[1–5] current leakage mechanisms that may limit the diode's dynamic impedance are thermal currents that include contribution from diffusion of minority carriers from quasi neutral regions to the junction and generation-recombination (g-r) of carriers in the depletion region, trap-assisted-tunnelling (TAT), band-to-band tunnelling (BTB), and ohmic currents.

A. Diffusion current (I_{df})

This component of the current is due to the transport of thermally generated minority carriers from the quasi-neutral

[a)]E mail: Vishnu_46@yahoo.com

regions to the junction by diffusion. In one sided n^+-p junction, the thermal diffusion current from the heavily doped side is negligibly small and the junction current of an epitaxial diode may be approximated to the minority carrier diffusion current from the lightly doped p-side,[6,7] i.e.

$$I_{df} = I_0\left[\exp\left(\frac{qV}{kT}\right) - 1\right], \tag{1}$$

$$I_0 = \frac{qAn_i^2}{N_A}\left[\frac{kT}{q}\frac{\mu_n}{\tau_n}\right]^{1/2}\tanh\left(\frac{t}{L_n}\right),$$

where N_A is the electrically active acceptor/hole concentration on the lightly doped p-side of the junction, n_i is the intrinsic carrier concentration, A is the junction area, τ_n is the minority carrier lifetime, μ_n is the minority carrier mobility, L_n is the minority carrier diffusion length, t is the thickness of the p-type base of the diode, and V is the bias voltage across the diode. T, q, and k are, respectively, the temperature, electronic charge, and Boltzmann constant.

B. Generation–recombination current (I_{gr})

In this type of current defects within the depletion region act as intermediate states (usually referred to as Shockley-Read or simply S-R centres) for the thermal generation and recombination of carriers. Sah, Noyce, and Shockley (SNS) analysed these currents and obtained the following equations:[8]

$$\mathbf{I_{g-r}} = \frac{\mathbf{qAn_iW}}{\sqrt{\tau_{n0}\tau_{p0}}}\frac{\sinh\left(-\frac{\mathbf{qV}}{\mathbf{2kT}}\right)}{\mathbf{q}\left[\frac{\mathbf{V_{bi}-V}}{\mathbf{2kT}}\right]}\mathbf{f(b)}, \tag{2}$$

where w is the depletion region width that is determined by

$$\mathbf{w} = \left[\frac{2\varepsilon_0\varepsilon_s(\mathbf{V_{bi}-V})(\mathbf{N_A+N_D})}{\mathbf{qN_AN_D}}\right]^{1/2},$$

where V_{bi} is the built-in voltage of the p-n junction, ε_0 is the permittivity of free space, ε_s is the static dielectric constant of HgCdTe, and N_D is the electron concentration on the heavily doped n-side of the junction. The function f (b) is defined by the following expression:

$$\mathbf{f(b)} = \int_0^\infty \frac{\mathbf{du}}{\mathbf{u^2+2bu+1}},$$

$$\mathbf{b} = \exp\left(-\frac{\mathbf{qV}}{\mathbf{2kT}}\right)\mathbf{cosh}\left[\frac{\mathbf{E_t-E_i}}{\mathbf{kT}}+\frac{1}{2}\ln\left(\frac{\tau_{p0}}{\tau_{n0}}\right)\right],$$

where $\tau_{n0}=\tau_{p0}$ is the effective lifetime in the depletion region, E_t is the bulk trap energy level, and E_i is the intrinsic energy level.

It is clear from the above description of diffusion and g-r currents that both of them are of thermal origin. In the present paper, the following simplified form is used to describe the combined contribution of both currents as one thermal current in a junction

$$I_{Th} = I_{sat}\left[\exp\left(\frac{qV}{\eta kT}\right) - 1\right]. \tag{3}$$

In Eq. (3), η is the ideality factor that assumes a value of unity in ideal diffusion current limited junctions. In junctions dominated by g-r current η will have a numerical value of 2. I_{sat} is the thermal saturation current of the junction diode that includes contributions from diffusion and g-r mechanisms.

C. TAT current

In this type of current minority carriers tunnel from the quasi-neutral region to the empty band states on the other side of the junction via trap sites present in the depletion region of the junction. In n^+-p junction, the major contribution of the TAT current is due to tunnelling of the electrons via trap levels to the conduction band on the n-side. This current (I_{TAT}) may be calculated using a simplified one dimensional model[9]

$$I_{TAT} = \frac{\pi^2q^2AN_Tm_e\xi M^2}{h^3(E_g-E_t)}\exp\left\{-\frac{8\pi(2m_e)^{\frac{1}{2}}(E_g-E_t)^{\frac{3}{2}}}{3qh\xi}\right\}, \tag{4}$$

where m_e is the effective mass of electrons in the conduction band, E_g is the band gap, M is the matrix element associated with the trap potential, h is the Planck's constant, ξ is the electric field strength across the depletion region, and E_t is the position of trap level in the band gap measured from the top of valence band on the p-side. The most commonly used value of the quantity M^2 (m/m_e) is 10^{-23} V^2 cm^3 for HgCdTe.

D. BTB current

At relatively high reverse bias voltages, the electrons directly tunnelling from the valence band on the p-side to the conduction band on the n-side under the influence of applied electric field "ξ" may give rise to the band-to-band tunnelling currents (I_{BTB}) in a junction. This current may be calculated by using the following simple equation:[1]

$$I_{BTB} = \frac{q^3A\xi V}{4\pi^2h^2}\left(\frac{2m_e}{E_g}\right)^{1/2}\exp\left\{-\frac{8\pi(2m_e)^{\frac{1}{2}}(E_g)^{\frac{3}{2}}}{3qh\xi}\right\}. \tag{5}$$

It may be noticed from the tunnelling current Eqs. (4) and (5) that the electric field responsible for the tunnelling of carriers is same and is given by

$$\xi = \left(\frac{qN_A(V_{bi}-V)}{2\varepsilon_s\varepsilon_0}\right)^{1/2},$$

$$\xi_{max} = \left(\frac{2qN_A(V_{bi}-V)}{\varepsilon_s\varepsilon_0}\right)^{1/2}.$$

Note that the electric field across the depletion width of the junction is variable from zero to ξ_{max}. Either an average value[10] $(\xi_{max}/2)$ or the maximum value[1] (ξ_{max}) of electric field strength has been used to calculate the tunnelling currents in an n^+-p junction. It is obviously an approximation.

E. Ohmic current (I_{Sh})

The current–voltage characteristics of a HgCdTe junction often exhibit an excess current component, a part of which can be modelled as an ohmic current that can be calculated by applying the Ohm's law, i.e.

$$I_{Sh} = \frac{V}{R_{Sh}} \tag{6}$$

where V is the applied bias voltage and R_{Sh} is the diode's shunt resistance. The surface leakage currents and the dislocations in the material, which intersect the junction,[11–14] are generally held responsible as a possible source of ohmic current. The contribution of ohmic currents from the two sources is not easily distinguishable. It is therefore modelled as gross contribution.

It is quite clear from Eqs. (1) to (6) that the investigation of leakage current mechanisms from dark current-voltage characteristic of a junction diode requires advance knowledge of a number of material and diode parameters. These include composition (x) of $Hg_{1-x}Cd_xTe$, acceptor/hole concentration (N_A) and electron mobility (μ_n) in p-type epitaxial base layer and its thickness t, donor/electron concentration (N_D) in the n-region, junction area (A), the lifetime of electrons (τ_n) in p-region, the effective lifetime ($\tau_{n0} = \tau_{p0} = \tau_0$) of electrical carriers in the depletion region, density of traps (N_T) contributing to the TAT currents. It is also known that the lifetime (τ_n) of minority carriers in p-region is dependent on temperature, dislocation density, and surface leakage current density. Most often the dependence of τ_n on temperature, dislocation density, and surface leakage current density is ignored due to the lack of desired information. Further known values of some of these parameters used in the modelling of electrical characteristic are based on the measured values on test samples. In addition, if the detector under investigation happens to be one of the diodes in an array, then the influence of neighbouring pixels (detectors) remains unknown. It will be now shown in Secs. IV–V that many of these problems may be avoided by investigating the illuminated current-voltage characteristic of given diode.

F. Illuminated current-voltage characteristics

The current transport in an illuminated junction diode is influenced due to the generation of photo-current (I_{Ph}) that consists of minority carriers. The net effect is to modify the forward characteristic of the diode that can be described by rewriting Eq. (3) in the following form:

$$I_{Th} = I_{sat}\left[\exp\left(\frac{qV}{\eta kT}\right) - 1\right] - I_{Ph}\,. \tag{7}$$

The illumination may be an external illumination or due to the background radiation received by the photodiodes.

In an illuminated diode, I-V characteristics of the diode get shifted along the current axis towards the negative values of the current by an amount equal to the value of photo-excited minority carrier current, I_{Ph}. Correspondingly, there is a shift in the forward characteristics along the voltage axis towards positive voltages by an amount equal to the open circuit voltage, V_{OC}. The following expression for V_{OC} is obtained by setting the net forward junction current (I_{Th}) equal to zero:

$$V_{OC} = \frac{\eta kT}{q} ln\left[\frac{I_{Ph}}{I_{sat}} + 1\right]. \tag{8}$$

In practice, the values of open circuit voltage V_{OC} and photo-current I_{Ph} are known from the illuminated I–V characteristic of the diode. It is then straight forward to estimate the thermal saturation current (I_{sat}) by fitting the forward characteristic of the diode to Eqs. (7) and (8). The ideality factor η may be treated as the variable parameter. In this method, care need to be exercised to include the series resistance of the diode by using the following expression:

$$V_{appl} = V + I_{TH}R_{sr},$$

where V_{appl} is the externally applied voltage, V is the voltage across diode, and R_{sr} is the series resistance of the diode.

IV. RESULTS AND DISCUSSIONS

A. Detectors in an area array

The typical measured I-V characteristics of a background illuminated diode at 80 K are shown in Figure 1. The experimental data are depicted by the open circles (O). Discussion of the results from the analysis of current–voltage characteristics of few diodes in an area array is presented below.

The forward current experimental data were subjected to the fitting to Eqs. (7) and (8) by treating the ideality factor η as variable parameters as already discussed in Sec. III. The continuous line marked with I_{Th} exhibits the thermal current, which provides an excellent fit to the forward characteristics after including the effect of series resistance of the diode. Most of the investigated diodes in the array exhibited

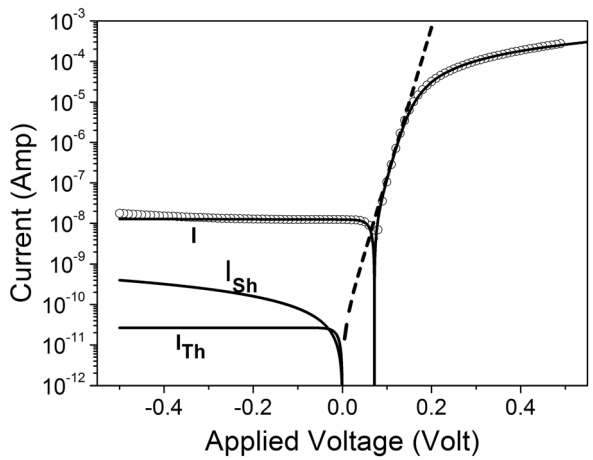

FIG. 1. Current–voltage characteristics of a MWIR HgCdTe diode at 80 K (diode number 11 in Table I) having dimensions of $40 \times 70\ \mu m^2$. Measured data are depicted by open circles. Lines in the figure correspond to calculated current contributions as marked on each of them. The resultant current, marked with I is the sum of thermal (I_{Th}), shunt (I_{Sh}), and photo-currents (I_{Ph}). Broken line shows the dark forward characteristic without including the contribution of series resistance.

TABLE I. Summary of open circuit voltage in few diodes of the array.

S.No.	Shunt resistance, "R_{Sh}" (Ohm)	Photo-current, I_{Ph} (Amp)	Thermal Saturation current, I_{sat} (Amp)	Open circuit voltage, V_{OC} (Volt)
1	1.88×10^{4}	…	…	Nil
2	2.00×10^{7}	1.29×10^{-8}	4.21×10^{-9}	.029
3	2.99×10^{7}	3.79×10^{-8}	6.87×10^{-11}	.074
4	3.53×10^{7}	6.32×10^{-9}	1.91×10^{-11}	.068
5	4.18×10^{7}	1.36×10^{-8}	3.16×10^{-11}	.070
6	4.90×10^{7}	3.69×10^{-8}	2.61×10^{-11}	.085
7	5.56×10^{7}	1.44×10^{-8}	2.20×10^{-11}	.076
8	7.52×10^{7}	1.39×10^{-8}	1.50×10^{-11}	.080
9	1.79×10^{8}	1.44×10^{-8}	2.20×10^{-11}	.076
10	3.50×10^{8}	1.19×10^{-8}	1.53×10^{-11}	.078
11	1.25×10^{9}	1.24×10^{-8}	2.67×10^{-11}	.072

excellent agreement with Eq. (7) for an ideality factor of 1.7. This value of η suggests that both the thermal mechanisms, namely, diffusion and g-r are contributing to the forward current of the diode.

The values of thermal saturation current I_{sat} obtained by fitting of the experimental data of some of the diodes in the array are shown in Table I. The photo-current I_{Ph} listed in column 3 of Table I is the observed shift of I–V characteristics along the current axis for $V = 0$. Similarly, the value of open circuit voltage V_{OC} listed in column 5 is the observed shift of I–V characteristics along the voltage axis. It is observed from Table I that I_{sat} and I_{ph} exhibit diode to diode variations. These variations may have arisen as a result of combined effect of several factors that include variations in the composition of base mercury cadmium telluride epitaxial layer, local variations in quantum efficiency, defect structure, semiconductor–passivant interface, and variations in the background radiation received by each diode. Current-voltage characteristics of diode at serial number 11 in Table I are shown in Figure 1. Broken line in this figure exhibits calculated forward dark characteristic without taking in to account the effect of series resistance of this diode.

Diode-to-diode variations in V_{OC} can be further understood by plotting Eq. (8) as shown in Figure 2. The

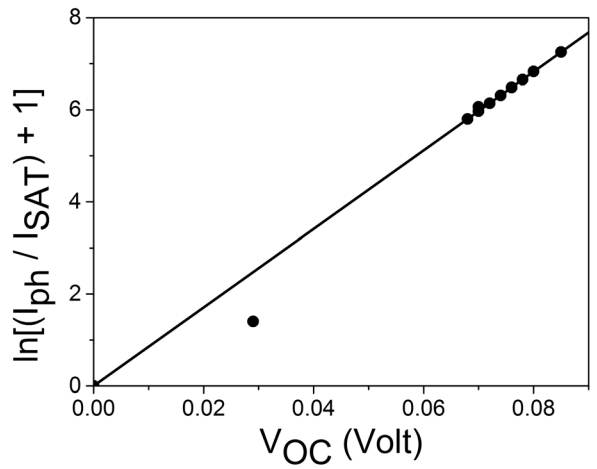

FIG. 2. Plot of Eq. (8) from the text to show that the observed V_{oc} of the diodes in the array follows well the predictions of the theory.

experimental points depicted by closed circles correspond to the diodes shown in Table I. It can be observed that open circuit voltage V_{OC} follows Eq. (8) very well. This means that the observed variations in V_{OC} are the result of several experimental factors as mentioned in the preceding paragraph. Deviation of open circuit voltage of the diode, at sr. No. 2, from the straight line in Figure 2 appears to be due to gross variations in the properties of the diode at this location. It is also evident from the higher numerical value of I_{sat} for this pixel. Note that the thermal saturation current of this pixel is higher by approximately two orders of magnitude. The ideality factor η for this pixel is also 3 as compared to 1.7 for other pixels. There were few diodes, such as listed at sr. No. 1 in Table I, which did not exhibit an open circuit voltage. These were the diodes that had very low shunt resistance. The effect of photo-excited current is masked by the high shunt current in this type of diodes. Other than the case of very low shunt resistance diodes, the open circuit voltage remains practically independent of variations in the shunt resistance as predicted by Eq. (8). The method of determining the shunt resistance of the diodes, as shown in column two of Table I, is discussed in the next paragraph with the discussion of the reverse bias characteristics.

The calculation of the current in the reverse bias region requires knowledge of the operative shunt resistance of the diode. The later can be obtained by computing the diode's dynamic resistance (dV/dI) as a function of bias voltage. The highest (peak) value of dynamic resistance is chosen as the operative shunt resistance of the diode. It may be worthwhile to point out here that dR/dV is zero at the peak of dynamic resistance versus voltage characteristic. Zero value of dR/dV indicates a resistance independent of the applied voltage meaning a resistance that obeys Ohm's law, i.e., ohmic shunt resistance R_{Sh} of the given diode.

In Figure 1, the continuous lines marked with I_{Th} and I_{Sh} are, respectively, the thermal and shunt current components. The resultant reverse bias current is marked with I $(= I_{Th} + I_{Sh} + I_{ph})$. It may be noted from Figure 1 that in relatively lower bias region, the calculated resultant reverse bias current is in very good agreement with the measured current shown by circles. At higher reverse bias voltages, the experimental data appear to indicate a higher measured current than the calculated current. This excess current in the reverse bias can be calculated by using following relation:

$$I_{excess} = I_{expt} - I_{Th} - I_{Sh} - I_{ph}. \quad (9)$$

According to our past knowledge,[1,3,4] the excess diode current in the low and medium reverse bias region is interpreted as the contribution of TAT mechanism. In the higher bias region, it is interpreted as the contribution from BTB mechanism. To be able to compare the variation of excess current with the tunnelling currents, the excess current obtained from Eq. (9) was subjected to an exponential fit as a function of reverse bias voltage. It was found that the excess current of all the investigated pixels listed in Table I can be very well described by an exponential function of the following form:

$$I_{excess} = I_{r0} + K_1 \exp(K_2 V), \quad (10)$$

where I_{r0}, K_1, and K_2 are the fitting parameters.

Figure 3 depicts the plot of calculated excess current for three pixels with variable shunt resistances. The excess current is shown by open symbols (squares, circles, and triangles). The continuous lines are the best exponential fits of the data to Eq. (10). The continuous line marked with the number 1 corresponds to the diode number 1, whose shunt resistance is lowest among all the pixels shown in Table I. Note that this pixel has the highest excess current. The excess current of this pixel has to be scaled down by a factor of 1000 to be able to plot it within in the scales of Figure 3. The line marked with number 11 corresponds to the diode number 11 with highest shunt resistance and lowest excess current. The line marked with the number 6 corresponds to diode number 6 with an intermediate shunt resistance, whose excess current too, is in the intermediate range.

Broken lines shown in Figure 3 show a comparison of calculated TAT current from Eq. (4) with the observed excess current of the respective diode. The agreement at highest bias voltage of 0.5 V was achieved by varying the trap density (N_T) contributing to trap-assisted-tunnelling current. It may be observed from Figure 3 that the calculated growth of the TAT current as a function of applied reverse bias voltage does not match with the measured growth of excess current in case of low shunt resistance diodes (pixels 6 and 1). The calculated TAT current shown by broken line is, however, not visible in case of high shunt resistance diode (pixel 11) as the difference in the current values depicted by broken and continuous lines is rather small and is therefore not visible on the scale shown in Figure 3. The difference in the variation of TAT and excess currents as a function of applied bias voltage appears to be an obvious consequence of different natures of the exponential functions in the two cases. Comparison of BTB current with the calculated excess current here appears to be irrelevant since the growth of BTB current is expected to be much slower than that of the TAT current.

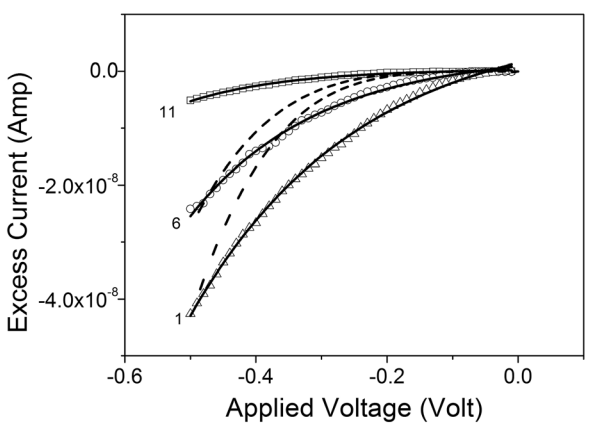

FIG. 3. Diode's reverse bias excess current (I_{excess}) versus applied bias voltage. Experimentally observed current in excess of the sum of calculated thermal, ohmic shunt, and photo currents is shown by the open symbols. Continuous lines are the exponential fits of Eq. (10) to the calculated excess current from Eq. (9). Line marked 1 corresponds to diode no. 1 with lowest shunt resistance (1.88×10^4 Ω). Line marked 6 corresponds to diode number 6 with an intermediate shunt resistance (4.9×10^7 Ω) and line marked 11 corresponds to diode number 11 with highest shunt resistance (1.25×10^9 Ω). Broken lines exhibit a comparison of growth of TAT current in the respective diodes, if TAT was one of the excess current contributing mechanisms.

Measured temperature dependence of excess current in one of the diode of the array is shown in Figure 4. Similar to Figure 3, the excess current at each temperature is shown by open symbols (square, circle, and triangle). Continuous lines are the best fit of excess current data to the exponential function defined in Eq. (10). Temperature of measurement is marked on the respective curve. The shunt resistance of the diode as determined from the maximum dynamic resistance of the diode is 2×10^9 Ω at 78 K, 9.5×10^8 Ω at 93 K, and 3.44×10^8 Ω at 130 K. It is observed that the growth of reverse bias excess current as a function of temperature of measurement has maintained the similar dependence on diode's shunt resistance as discussed in the preceding paragraph. The calculation of the growth of TAT current, shown by broken lines in Figure 3, is not considered necessary in this case as the contribution from TAT currents is expected to decrease with the increase in temperature. It is also well known from past investigations[15] that TAT currents play a dominant role at low temperatures below 70 K.

Some of the observations that emerge from the above discussions are: (i) Miss-match between the growth rates of excess current and TAT current as a function of applied bias voltage suggest that tunnelling mechanisms are not the major contributing mechanisms to the excess current of the investigated diodes. (ii) The dependence of excess current on the ohmic shunt resistance indicates a close relationship of excess current with the sources of ohmic current in the diode. (iii) The exponential growth of the excess current with the applied reverse bias voltage combined with the fact that higher excess current lead to its faster growth rate points out towards the soft breakdown of diodes.

Some of the past observations of the soft breakdown of the diodes with enhanced reverse bias leakage currents and having a close link with the sources of ohmic current in semiconductor diodes are discussed in the following paragraph.

It is well known that the surface leakage currents and the line dislocations[11–14] that intersect the junction are the

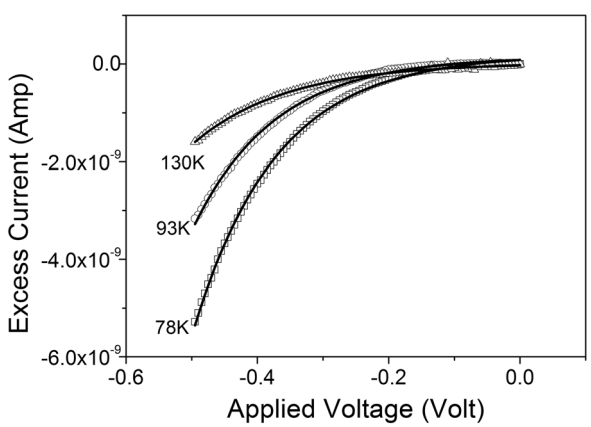

FIG. 4. Excess current (I_{excess}) versus reverse bias voltage as a function of measurement temperature. Open symbols show the calculated current from Eq. (9). The temperature of measurement is marked on the respective curve. Continuous lines are the exponential fits of the calculated excess current to Eq. (10).

two possible sources of ohmic currents in a diode. In this connection, it will be worthwhile to mention the observations of avalanche breakdown micro-plasmas in Si diodes,[16] which were closely associated with the dislocations. Similar observations of excess leakage currents have also been reported in 4H-SiC p^+ n junction diodes.[17] Stress field induced band gap narrowing in the vicinity of line dislocations is another possibility that may give rise to excess leakage currents due to Zener like tunnelling[18] along the dislocations in narrow band gap material HgCdTe diodes. Breakdown of a diode along the surface leakage current path[19] may be another possible reason for giving rise to excess reverse bias current/soft electrical characteristics of the diode.

V. SUMMARY AND CONCLUSIONS

In this work, the (background) illuminated I-V characteristics of MWIR HgCdTe diodes in a 2-D array were investigated from −0.5 to 0.5 V. The thermal saturation current of the diode was estimated from the observed photocurrent and open circuit voltage without using any advance knowledge of material and device parameters. The ideality factor (η) of the diode was treated as the fitting parameter. Based on the estimates of η (1.7 in the present case), it was concluded that both diffusion and g-r mechanisms were contributing to the thermal current. The ohmic current contribution was estimated by assuming the maximum dynamic impedance (dR/dV) of the diode as shunt resistance. The measured reverse bias current in excess of the sum of thermal current, photocurrent, and ohmic shunt current was investigated as a function of reverse bias voltage. It has been found that the tunnelling mechanisms (TAT and BTB) were not the contributing mechanisms in the investigated diodes. The exponential growth of the excess current as a function of the reverse bias voltage combined with the fact that higher excess current leads to its faster growth rate was interpreted as an indication of the soft breakdown of the diodes. The excess current exhibited a close relationship with the sources of ohmic current in the diode. Some of the previously reported possibilities that may give rise to the kind of excess current reported in the present paper have been mentioned in support of the presented results.

In conclusion, this paper has presented in a new approach to investigate leakage current mechanisms from illuminated I–V characteristic of a diode. The advantage of the new approach is obvious for evaluation of diodes in an array environment. Precise knowledge of material parameters at the location of the diode, influence of neighbouring diodes and the temperature dependence of the various parameters is no longer a requirement in this method. Another interesting conclusion that emerges from this investigation is the importance of minimizing the sources of ohmic currents in the diode array to realise the ideal diffusion current limited diodes with high zero-bias dynamic impedance suitable for advanced infrared detector systems.

ACKNOWLEDGMENTS

I am thankful to the Director Solid State Physics Laboratory, Lucknow Road, Timarpur Delhi 110054 for the award of the project under which this work had been performed. My grateful thanks are also due to Professor Vikram Kumar of Indian Institute of Technology Delhi, India for critical reading of the manuscript of this paper and making several valuable suggestions. The author is the principal investigator of the project awarded by Solid State Physics Laboratory to Institute of Defence Scientists and Technologists, Delhi.

[1]A. S. Gilmore, J. Bangs, and A. Gerrish, Proc. SPIE **5563**, 46 (2004).
[2]A. Zemel, I. Lukomsky, and E. Weiss, J. Appl. Phys. **98**, 054504 (2005).
[3]W. D. Hu, X. S. Chen, F. Yin, Z. J. Quan, Z. H. Ye, X. N. Hu, Z. F. Li, and W. Lu, J. Appl. Phys. **105**, 104502 (2009).
[4]J. Wang, X. Chen, W. D. Hu, Z. Ye, C. Lin, X. N. Hu, J. Guo, F. Xie, J. Zhou, J. Liang, X. F. Wang, and W. Lu, Infrared Phys. Technol. **61**, 157 (2013).
[5]V. Gopal, X. H. Xie, Q. J. Liao, and X. N. Hu, Infrared Phys. Technol. **64**, 56 (2014).
[6]M. B. Reine, A. K. Sood, and T. J. Tredwell, in *Photovoltaic Infrared Detectors*, edited by R. K. Willardson and A. C. Beer (Academic Press, NY, 1983).
[7]In "Photovoltaic detectors," *Infrared Photon Detectors*, edited by A. Rogalski (SPIE Optical Engineering Press, Bellingham, 1995).
[8]C. T. Sah, R. N. Noyce, and W. Shockley, Proc. IRE **45**, 1228 (1957).
[9]J. Y. Wong, IEEE ED **27**, 48 (1980).
[10]V. Gopal and V. Dhar, IEEE ED **33**, 1489 (1986).
[11]S. M. Johnson, D. R. Rhiger, J. P. Rosbeck, J. M. Peterson, S. M. Taylor, and M. E. Boyd, J. Vac. Sci. Technol. B **10**, 1499 (1992).
[12]I. M. Baker and C. D. Maxey, J. Electron. Mater. **30**, 682 (2001).
[13]V. Gopal and S. Gupta, IEEE ED **50**, 1220 (2003).
[14]V. Gopal and S. Gupta, IEEE ED **51**, 1078 (2004).
[15]A. Rogalski, J. Appl. Phys. **93**, 4355 (2003).
[16]A. G. Chynoweth and G. L. Pearson, J. Appl. Phys. **29**, 1103 (1958).
[17]P. G. Neudeck, W. Huang, and M. Dudley, IEEE ED **46**, 478 (1999).
[18]R. K. Sharma, V. Gopal, R. S. Saxena, R. K. Bhan, and R. Pal, "On the role of dislocations in influencing the electrical properties of HgCdTe photodiodes," Proc. SPIE **8012**, 80123A (2011).
[19]V. Gopal, R. J. Westerhout, and L. Faraone, Infrared Phys. Technol. **51**, 532 (2008).